JGP Journal of General Physiology

RESEARCH ARTICLE

Splicing of an automodulatory domain in $Ca_V1.4$ Ca^{2+} channels confers distinct regulation by calmodulin

Brittany Williams[1,2,3], Françoise Haeseleer[6], and Amy Lee[1,2,3,4,5]

Ca^{2+} influx through $Ca_V1.4$ L-type Ca^{2+} channels supports the sustained release of glutamate from photoreceptor synaptic terminals in darkness, a process that is critical for vision. Consistent with this role, $Ca_V1.4$ exhibits weak Ca^{2+}-dependent inactivation (CDI)—a negative feedback regulation mediated by Ca^{2+}-bound calmodulin (CaM). CaM binds to a conserved IQ domain in the proximal C-terminal domain of Ca_V channels, but in $Ca_V1.4$, a C-terminal modulatory domain (CTM) disrupts interactions with CaM. Exon 47 encodes a portion of the CTM and is deleted in a $Ca_V1.4$ splice variant ($Ca_V1.4\Delta ex47$) that is highly expressed in the human retina. $Ca_V1.4\Delta ex47$ exhibits CDI and enhanced voltage-dependent activation, similar to that caused by a mutation that is associated with congenital stationary night blindness type 2, in which the CTM is deleted (K1591X). The presence of CDI and very negative activation thresholds in a naturally occurring variant of $Ca_V1.4$ are perplexing considering that these properties are expected to be maladaptive for visual signaling and result in night blindness in the case of K1591X. Here we show that $Ca_V1.4\Delta ex47$ and K1591X exhibit fundamental differences in their regulation by CaM. In $Ca_V1.4\Delta ex47$, CDI requires both the N-terminal (N lobe) and C-terminal (C lobe) lobes of CaM to bind Ca^{2+}, whereas CDI in K1591X is driven mainly by Ca^{2+} binding to the C lobe. Moreover, the CaM N lobe causes a Ca^{2+}-dependent enhancement of activation of $Ca_V1.4\Delta ex47$ but not K1591X. We conclude that the residual CTM in $Ca_V1.4\Delta ex47$ enables a form of CaM N lobe regulation of activation and CDI that is absent in K1591X. Interaction with the N lobe of CaM, which is more sensitive to global elevations in cytosolic Ca^{2+} than the C lobe, may allow $Ca_V1.4\Delta ex47$ to be modulated by a wider range of synaptic Ca^{2+} concentrations than K1591X; this may distinguish the normal physiological function of $Ca_V1.4\Delta ex47$ from the pathological consequences of K1591X.

Introduction

Voltage-gated Ca_V Ca^{2+} channels are essential regulators of Ca^{2+} signaling and are composed of a pore-forming α_1 subunit and auxiliary β and $\alpha_2\delta$ subunits. The pharmacological and biophysical properties of Ca_V subunits are largely determined by the α_1 subunit (Simms and Zamponi, 2014). In contrast to the tremendous diversity of genes encoding voltage-gated K_V K^+ channels, the Ca_V α_1 subunit in mammals is encoded by only 10 different genes (Yu et al., 2005). However, each α_1 gene can give rise to thousands of splice variants, the exact complement of which depends on the types of splicing factors that are expressed (Lipscombe et al., 2013). Combined with the splice variation affecting β and $\alpha_2\delta$ subunits (Buraei and Yang, 2013; Dolphin, 2013), the vast molecular diversity of α_1 splice isoforms helps tailor Ca_V channel properties according to a defined cellular and/or developmental context.

Among the cytoplasmic regions of the Ca_V α_1 subunit, the C-terminal domain (CTD) is the largest and subject to significant splice variation that can alter channel function. For example, the inclusion of either of two mutually exclusive exons (37a and 37b) in the proximal C-terminal domain (pCTD) of $Ca_V2.2$ affects the voltage dependence of channel inhibition by G protein–coupled receptors (Raingo et al., 2007), and the role of $Ca_V2.2$ in mediating the analgesic effects of morphine in spinal nociceptors (Andrade et al., 2010). Alternative splicing of the analogous exons in $Ca_V2.1$ (P/Q-type) channels as well as an exon in the distal CTD transforms the Ca^{2+}-sensitivity of Ca^{2+}/calmodulin (CaM)-dependent facilitation of these channels (Chaudhuri et al., 2004). The expression of these $Ca_V2.1$ splice variants is developmentally regulated in ways that may support the maturation of the firing properties of cerebellar Purkinje neurons (Chaudhuri et al., 2005).

In the retina, $Ca_V1.4$ L-type channels are localized in the synaptic terminals of rod and cone photoreceptors, where they mediate

[1]Department of Molecular Physiology and Biophysics, University of Iowa, Iowa City, IA; [2]Interdisciplinary Graduate Program in Neuroscience, University of Iowa, Iowa City, IA; [3]Iowa Neuroscience Institute, University of Iowa, Iowa City, IA; [4]Department of Otolaryngology Head-Neck Surgery, University of Iowa, Iowa City, IA; [5]Department of Neurology, University of Iowa, Iowa City, IA; [6]Department of Physiology and Biophysics, University of Washington, Seattle, WA.

Correspondence to Amy Lee: amy-lee@uiowa.edu.

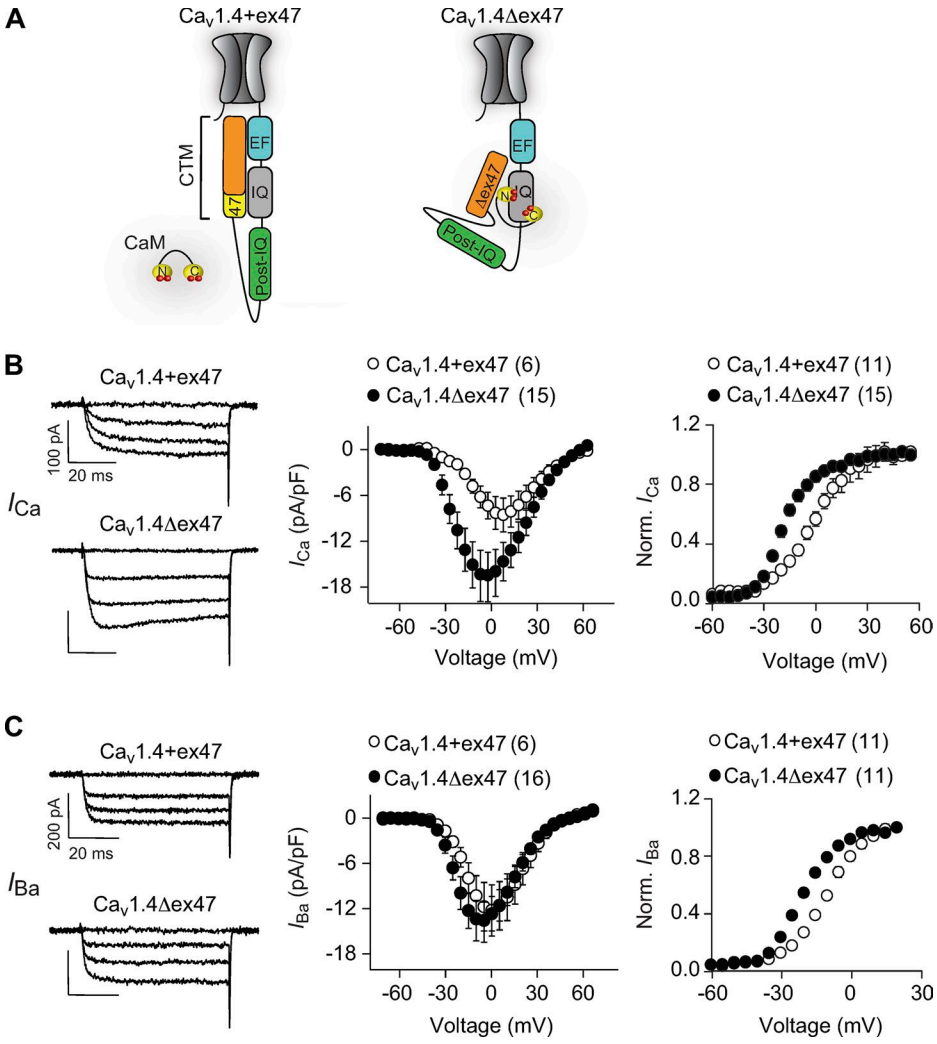

Figure 1. **Deletion of exon 47 promotes CDEA of $Ca_v1.4\Delta ex47$. (A)** Schematic showing the proposed function of the CTM modulating CaM interactions with $Ca_v1.4$ + ex47 and $Ca_v1.4\Delta ex47$. **(B and C)** Representative family of traces (left panels) and I–V plots for I_{Ca} (B) and I_{Ba} (C) in cells transfected with $Ca_v1.4$ + ex47 or $Ca_v1.4\Delta ex47$. Currents were evoked by 50-ms depolarizations to various voltages. Current amplitudes were normalized to cell capacitance and plotted against test voltage (middle panels). Tail current amplitudes were normalized to −60 mV for I_{Ca} (Norm. I_{Ca}) and −20 mV for I_{Ba} (Norm. I_{Ba}) and plotted against test voltage (right panels). Here and in all figures, parentheses indicate numbers of cells. Error bars represent mean ± SEM.

the tonic release of glutamate necessary for the encoding of light responses (McRory et al., 2004; Mansergh et al., 2005; Specht et al., 2009; Liu et al., 2013). Unlike $Ca_v1.2$ and $Ca_v1.3$ channels, $Ca_v1.4$ exhibits little Ca^{2+}-dependent inactivation (CDI) in heterologous expression systems (Baumann et al., 2004; McRory et al., 2004; Singh et al., 2006; Wahl-Schott et al., 2006). CDI is a hallmark feature of most Ca_v1 and Ca_v2 channels and depends on CaM binding to a consensus IQ domain in the pCTD of the channel (Ben-Johny and Yue, 2014). CDI of $Ca_v1.4$ is blunted by a CTM that competes with CaM interactions with the channel (Singh et al., 2006; Liu et al., 2010; but see Wahl-Schott et al., 2006; Griessmeier et al., 2009).

Numerous $Ca_v1.4$ splice variants have been identified in human retina with variations affecting the CTM. For example, $Ca_v1.4$ variants containing the alternately spliced exon 43 ($Ca_v1.4$ + ex43) are prematurely truncated, resulting in removal of the CTM. Like channels in which the entire CTM is deleted (Singh et al., 2006; Wahl-Schott et al., 2006), $Ca_v1.4$ + ex43 exhibits robust CDI as well as a negative shift in the half-maximal voltage (V_h; Tan et al., 2012) of channel activation. Strong CDI and a hyperpolarized V_h are also caused by a mutation (K1591X) associated with congenital stationary night blindness type 2 (CSNB2; Strom et al., 1998), which deletes the CTD distal to the IQ domain, including the CTM (Singh et al., 2006). The physiological significance of naturally occurring splice variants with properties similar to disease-causing mutant channels is unclear.

We previously characterized a splice variant of $Ca_v1.4$ L-type channels lacking exon 47 ($Ca_v1.4\Delta ex47$), which encodes part of the CTM. $Ca_v1.4\Delta ex47$ is highly expressed in human retina and exhibits prominent CDI as well as a negative shift in V_h (Haeseleer et al., 2016). These properties suggest that deletion of exon 47 might enable CaM regulation by altering or preventing the CTM interaction with the pCTD, but mechanistic details are lacking. Moreover, it is not known how deletion of exon 47 promotes voltage-dependent activation of $Ca_v1.4\Delta ex47$. Considering that alternative splicing of Ca_v channels can affect the functional impact of disease-causing

Table 1. **Parameters for voltage-dependent activation and current density from I–V data**

Construct	Peak current density (pA/pF)	P value	*Vh*	P value versus $Ca_v1.4\Delta ex47$	*k*	P value
I_{Ca}						
$Ca_v1.4$ + ex47	−8 ± 1.0	0.043	7 ± 0.7	<0.001	−9 ± 0.4	0.160
$Ca_v1.4\Delta ex47$	−17 ± 1.0	—	−1 ± 1.3	—	−10 ± 0.2	—
$Ca_v1.4\Delta ex47$ + CaM_{12}	−6 ± 0.83	0.018	6 ± 1.4	<0.001	−10 ± 0.2	0.600
$Ca_v1.4\Delta ex47$ + CaM_{34}	−12 ± 1.0	0.386	−2 ± 1.4	0.629	−8 ± 0.3	0.005
I_{Ba}						
$Ca_v1.4$ + ex47	−12 ± 3.3	0.958	−6 ± 1.0	<0.001	−8 ± 0.3	0.133
$Ca_v1.4\Delta ex47$	−12 ± 2.3	—	−14 ± 1.1	—	−7 ± 0.2	—
$Ca_v1.4\Delta ex47$ + CaM_{12}	−13 ± 2.5	0.230	−15 ± 1.1	0.728	−7 ± 1.5	0.448
$Ca_v1.4\Delta ex47$ + CaM_{34}	−7 ± 1.3	0.714	−18 ± 1.9	0.946	−8 ± 1.8	0.042

V_h and k values (mean ± SEM) were determined from Boltzmann fits of I–V data. Peak current density was defined as the maximum current amplitude normalized to the cell capacitance. P values indicate comparisons with $Ca_v1.4\Delta ex47$ and were determined by Student's *t* test.

mutations (Adams et al., 2009), a thorough analysis of the properties of $Ca_v1.4\Delta ex47$ is important for understanding how *CACNA1F* mutations may cause vision impairment in humans.

Here, we report a dual role for CaM in regulating both CDI and voltage-dependent activation of $Ca_v1.4\Delta ex47$. In addition, we demonstrate distinct routes whereby the individual Ca^{2+} binding lobes of CaM regulate K1591X and $Ca_v1.4\Delta ex47$. Our findings highlight the versatility of CaM as a regulator of Ca_v channels, and how modulation by CaM can be affected by naturally and pathologically occurring variations in the channel protein.

Materials and methods

Complementary DNAs (cDNAs) and molecular biology

The following cDNAs were used: $Ca_v1.4$ (GenBank no. AF201304), $\beta_{2\times13}$ (GenBank no. AF465485), and $\alpha_2\delta_4$ (GenBank no. NM_172364) in pcDNA3.1 (Lee et al., 2015); CaM deficient in Ca^{2+} binding to the N-terminal lobe (N lobe; CaM_{12}), CaM deficient in Ca^{2+} binding to the C-terminal lobe (C lobe; CaM_{34}), CaM deficient in Ca^{2+} binding to both the N lobe and C lobe (CaM_{1234}; GenBank no. NM_017326.3) in pcDNA6V5-His (Lee et al., 2003); β_{2a} (GenBank no. M80545.1). In $Ca_v1.4\Delta ex47$, alanine substitutions at residues I1588A, Q1589A, D1590A, Y1591A, and F1592A (5A), and F1582A, Y1583A, and F1586A (3A), were generated with primers incorporating the mutations (5′-CTACGCCACATTTCTGGCCGC GGCCGCTGCCCGCAAATTCCGG-3′ for 5A, 5′-GTCACCGTGGGC AAAGCCGCCGCCACAGCTCTGATCCAGGACTATTTCCGC-3′ for 3A, respectively) using the QuikChange Lightning Multi Site-directed Mutagenesis kit (Agilent) according to the manufacturer's protocol. The 3A mutations were generated in K1591X-3A with the HiFi DNA Assembly Cloning System (New England Biolabs) using K1591X as a PCR template and a gBlock containing the 3A mutations (Integrated DNA Technologies). All constructs were verified by DNA sequencing before use.

Cell culture and transfection

Human embryonic kidney 293 T cells (CRL-3216, Research Resource Identifier; CVCL_0063, American Type Culture Collection) were cultured in Dulbecco's modified Eagle's medium (Life Technologies) with 10% FBS (Atlantic Biologicals) at 37°C in 5% CO_2. At 70–80% confluence, the cells were cotransfected with cDNAs encoding human $Ca_v1.4$ α_1 (1.8 µg; $Ca_v1.4$ + ex47, $Ca_v1.4\Delta ex47$, K1591X, or 5A or 3A mutants), $\beta_{2\times13}$ (0.6 µg), $\alpha_2\delta_4$ (0.6 µg), and enhanced GFP in pEGFP-C1 (0.1 µg) using FuGENE 6 transfection reagent (Promega) according to the manufacturer's protocol. For some experiments, cells were cotransfected with cDNAs encoding CaM_{12}, CaM_{34}, or CaM_{1234} (1 µg each) or pcDNA3.1 (1 µg) as a control. Cells treated with the transfection mixture were incubated at 37°C for 24 h. After 24 h, cells were incubated at 30°C for at least 24 h before whole-cell patch clamp recordings.

Electrophysiology

Whole-cell patch clamp recordings were performed at room temperature between 48 and 72 h after transfection with an EPC-9 patch clamp amplifier operated by either Patchmaster software (HEKA Elektronik). External recording solutions consisted of (in mM) Tris (140), $CaCl_2$ or $BaCl_2$ (20), and $MgCl_2$ (1). Internal recording solution consisted of (in mM) NMDG (140), HEPES (10), $MgCl_2$ (2), Mg-ATP (2), and EGTA (5). The pH of external and internal recording solutions was adjusted to 7.3 with methanesulfonic acid. Pipette resistances were typically 2–4 MΩ in the bath solution, and series resistance compensated up to 70%. Leak subtraction was conducted using a P/−4 protocol.

To measure current density, Ca^{2+} and Ba^{2+} currents (I_{Ca}, I_{Ba}) were evoked by 50-ms pulses from −80 mV to various voltages and normalized to the cell capacitance. To characterize voltage-dependent activation, currents were evoked by 10-ms steps from −80 mV to various voltages. Tail currents were measured upon repolarization to −60 mV for 2 ms. For I_{Ca}, tail current amplitudes were normalized to that at +60 mV. Because of a decline in the amplitude of I_{Ba} tail currents at positive voltages, tail currents for I_{Ba} were normalized to that at +20 mV. I–V data were fitted with single or double Boltzmann equations: $I = I_{max} / [1 + \exp(V - V_h) / k)]$ or $I = I_{max} / [1 + \exp(V - V_{h1}) / k_1] + I_{max} / [1 + \exp(V - V_{h2}) / k_2]$, where I_{max} is the maximal current, V is the test voltage, V_h is the half-maximal activation, and k is the slope

Table 2. **Parameters for voltage-dependent activation from tail I–V data**

Construct	*Vh* (mV)	P value versus $Ca_v1.4$ + ex47	P value versus $Ca_v1.4\Delta ex47$	P value versus K1591X	*k*	P value versus $Ca_v1.4$ + ex47	P value versus $Ca_v1.4\Delta ex47$	P value versus K1591X
I_{Ca}								
$Ca_v1.4$ + ex47	−3 ± 1.5	—	—	—	−11 ± 1.0	—	—	—
$Ca_v1.4\Delta ex47$	−18 ± 1.0	<0.001[a]	—	—	−7 ± 1.2	<0.001[b]	—	—
$Ca_v1.4\Delta ex47$ + CaM_{34}	−13 ± 2.2	<0.001[c]	0.144[c]	—	−7 ± 1.1	0.011[c]	>0.999[c]	—
$Ca_v1.4\Delta ex47$-5A	−7± 0.2.4	0.165[c]	0.005[c]	—	−11 ± 0.4	>0.999[d]	0.004[d]	—
K1591X	−22 ± 1.0	0.001[c]	0.933[c]	—	−9± 0.6	0.264[d]	0.369[d]	—
K1591X + CaM_{12}	−20 ± 0.7	0.001[d]	—	>0.999[d]	−8 ± 0.5	0.038[d]	—	>0.999[d]
K1591X-3A	−16 ± 1.2	<0.001[d]	—	0.064[d]	−10 ± 0.6	>0.999[d]	—	>0.999[d]
I_{Ba}								
$Ca_v1.4$ + ex47	−10 ± 1.0	—	—	—	−8 ± 0.4	—	—	—
$Ca_v1.4\Delta ex47$	−20 ± 1.0	<0.001[a]	—	—	−7 ± 0.3	0.044[a]	—	—
$Ca_v1.4\Delta ex47$ + CaM_{12}	−20 ± 1.3	<0.001[c]	0.966[c]	—	−8 ± 0.5	0.735[c]	0.029[c]	—
$Ca_v1.4\Delta ex47$ + CaM_{34}	−23 ± 1.5	<0.001[c]	0.330[c]	—	−7 ± 1.0	0.866[c]	0.866[c]	—
$Ca_v1.4\Delta ex47$-5A	−17± 1.6	0.034[c]	0.477[c]	—	−8 ± 1.1	0.792[c]	0.196[c]	—
$Ca_v1.4\Delta ex47$-3A	−20± 2.0	<0.001[c]	0.993[c]	—	−7 ± 1.0	0.970[c]	0.860[c]	—

V_h and *k* values (mean ± SEM) were determined from single Boltzmann fits of the tail I–V data as indicated in the "Methods" section.
[a]Student's *t* test.
[b]Mann–Whitney test.
[c]One-way ANOVA with Tukey's multiple comparison test.
[d]Kruskal–Wallis test and post hoc Dunn's multiple comparison test.

factor. To measure CDI, currents were evoked by 1-s depolarizations from −80 mV to various voltages. Fractional I_{Ca} or I_{Ba} was defined as the residual current amplitude at the end of the pulse normalized to the peak current amplitude. Fractional CDI was the difference in fractional I_{Ca} at −20 mV and mean fractional I_{Ba} at −20 mV, except where indicated. Kinetic parameters for I_{Ca} inactivation were obtained by fitting with a double exponential function ($y_0 + A_{fast}$ [exp $(-t/\tau_{fast})$] + A_{slow} [exp $(-t/\tau_{fast})$]), where y_0 is the offset (asymptote), τ_{fast} and τ_{slow} are the time constants, and A_{fast} and A_{slow} are the relative amplitudes of fast and slow components of inactivation.

Data were analyzed offline with Igor Pro software (Wavemetrics). Statistical analysis was performed using SigmaPlot (Systat Software Inc.) or GraphPad Prism software. The data were initially analyzed for normality using the Shapiro–Wilk or D'Agostino–Pearson omnibus test. For parametric data, significant differences were determined by Student's *t* test or ANOVA with post hoc Dunnett or Tukey test. For nonparametric data, Kruskal–Wallis and post hoc Dunn's tests were used. Data were incorporated into figures using GraphPad, SigmaPlot, and Adobe Illustrator software. All averaged data represent the mean ± SEM from at least three independent transfections.

Online supplemental material

Fig. S1 shows that CaM mutants do not impact I_{Ca} density or voltage-dependent activation of $Ca_v1.4$ + ex47. Fig. S2 shows the lack of CDI in a subset of cells transfected with $Ca_v1.4\Delta ex47$-3A in which very slow activation was observed.

Results

Deletion of exon 47 causes a Ca^{2+}-dependent enhancement in activation of $Ca_v1.4$

Because $Ca_v1.4\Delta ex47$ is expressed in human but not mouse retina (Lee et al., 2015), we focused on $Ca_v1.4$ channels containing auxiliary $Ca_v\beta$ and $\alpha_2\delta$ subunits that predominate in the human retina—$\beta_{2\times13}$ (a splice variant of $Ca_v\beta_2$) and $\alpha_2\delta_4$ (Lee et al., 2015). We compared the properties of $Ca_v1.4$ + ex47 and $Ca_v1.4\Delta ex47$ (Fig. 1 A) cotransfected with $\beta_{2\times13}$ and $\alpha_2\delta_4$ in whole-cell patch clamp recordings of human embryonic kidney 293 T cells. Due to our interests in comparing CDI, voltage protocols were performed with either Ca^{2+} or Ba^{2+} as the permeant ion. In agreement with our previous study (Haeseleer et al., 2016), I_{Ca} mediated by $Ca_v1.4\Delta ex47$ activated at more negative voltages than $Ca_v1.4$ + ex47. While this was also seen for Ba^{2+} currents (I_{Ba}), the doubling in current density for I_{Ca} in cells transfected with $Ca_v1.4\Delta ex47$ was not observed for I_{Ba} (Fig. 1, B and C; and Table 1). Since parameters of voltage-dependent activation obtained from I–V relationships may be affected by the change in driving force that occurs with different test voltages, we also analyzed the voltage dependence of the tail current measured upon repolarization from the test voltage to a fixed voltage (−60 mV). The amplitude

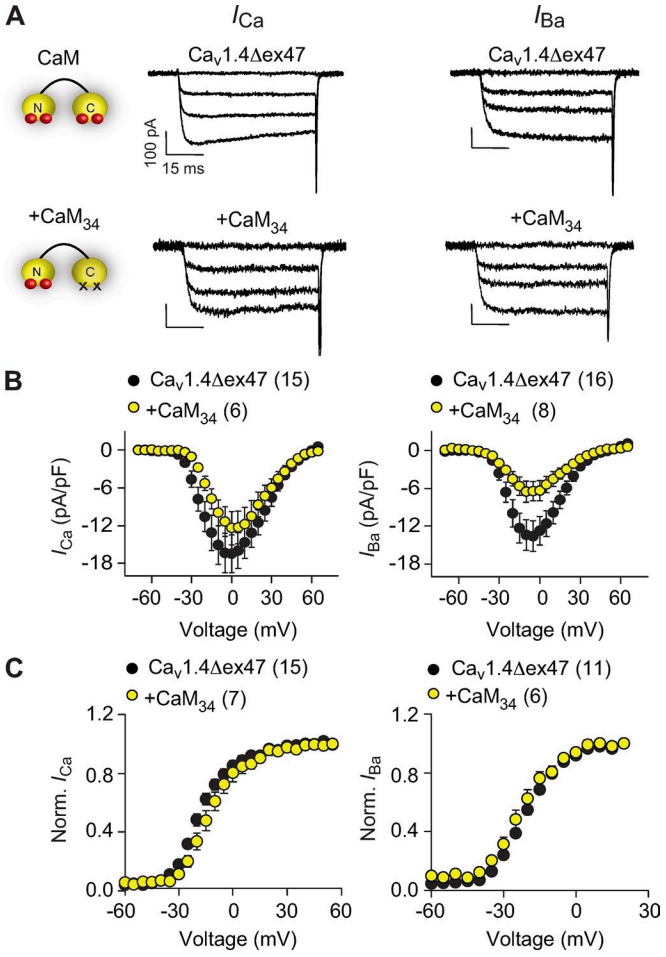

Figure 2. **CaM C lobe does not mediate CDEA of $Ca_v1.4\Delta ex47$. (A)** CaM and mutant CaM with deficient Ca^{2+} binding to C lobe (left). Representative traces for I_{Ca} and I_{Ba} in cells transfected with $Ca_v1.4\Delta ex47$ ± CaM_{13} (right). **(B and C)** Same as in Fig. 1, B and C, except in cells transfected with $Ca_v1.4\Delta ex47$ ± CaM_{34}. Error bars represent mean ± SEM.

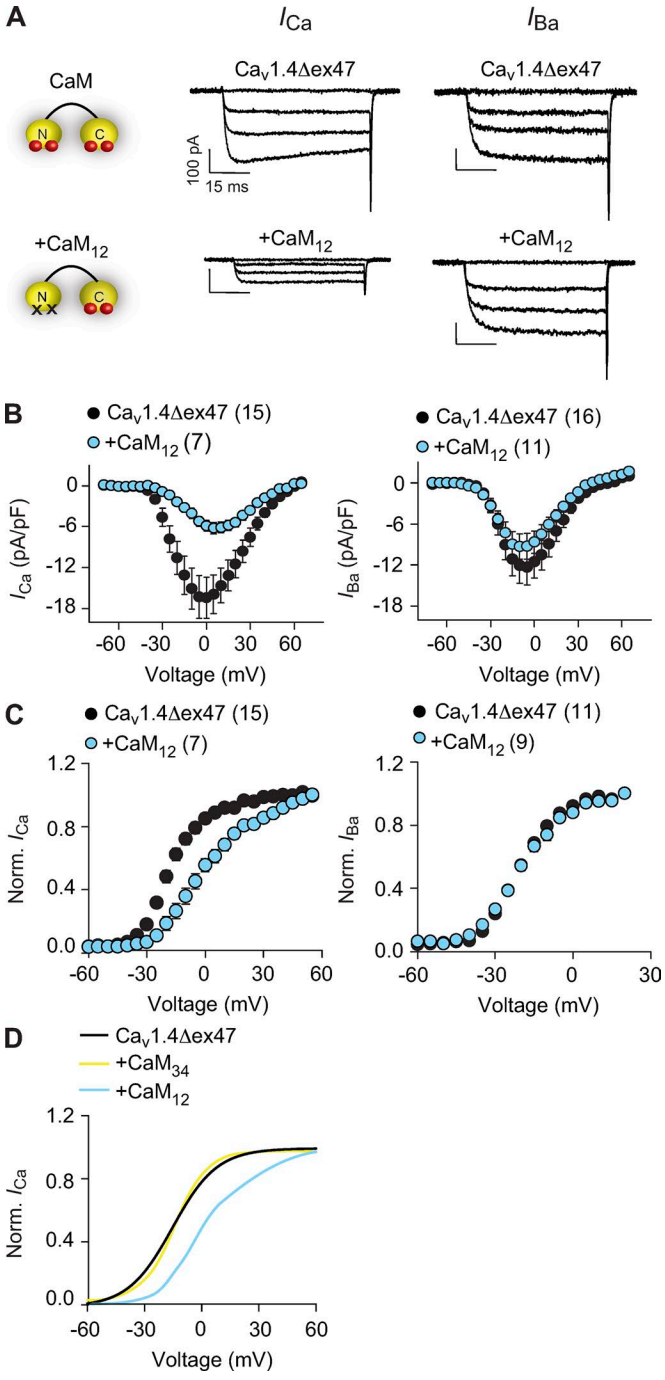

Figure 3. **CaM N lobe mediates CDEA of $Ca_v1.4\Delta ex47$. (A)** CaM and mutant CaM with deficient Ca^{2+} binding to N lobe (left). **(B and C)** Same as in Fig. 2, B and C, except in cells transfected with $Ca_v1.4\Delta ex47$ ± CaM_{12}. **(D)** Boltzmann fits of the averaged I_{Ca} data in C (double Boltzmann fit for $Ca_v1.4\Delta ex47$ + CaM_{12}). The single Boltzmann fit of I_{Ca} data in Fig. 2 B for $Ca_v1.4\Delta ex47$ + CaM_{34} is overlaid for comparison. Error bars represent mean ± SEM.

of the tail current reflects the number of channels open during the test pulse and rises sigmoidally with the test voltage. Boltzmann fits of these data indicated a significant hyperpolarizing shift in the activation curve, and steepening of the slope (k), for $Ca_v1.4\Delta ex47$ compared with $Ca_v1.4$ + ex47. While these alterations in tail I–V curves were found for both I_{Ca} and I_{Ba} (Fig. 1, B and C; and Table 2), the difference in V_h and k values between $Ca_v1.4\Delta ex47$ and $Ca_v1.4$ + ex47 was significantly larger for I_{Ca} than for I_{Ba} (ΔV_h = −15 ± 1.0 mV for I_{Ca} versus ΔV_h = −10 ± 1.1 mV for I_{Ba}; P = 0.003 by t test; Δk = −3 ± 0.5 for I_{Ca} versus Δk = −1 ± 0.2 for I_{Ba}; P < 0.001 by t test). Therefore, in addition to enhancing voltage-dependent activation of I_{Ba}, deletion of exon 47 causes a Ca^{2+}-dependent enhancement of activation (CDEA) of I_{Ca}.

CDEA is mediated by the N lobe of CaM

To investigate the mechanism underlying CDEA of $Ca_v1.4\Delta ex47$, we considered CaM because of its role in Ca^{2+}-dependent modulation of Ca_v channels (Ben-Johny and Yue, 2014). For $Ca_v1.2$, Ca^{2+} binding to the pairs of EF-hand motifs in the C lobe and N lobe of CaM is required for CDI (Peterson et al., 1999) and CDF (Van Petegem et al., 2005), respectively. CaM mutants deficient in Ca^{2+} binding to the N lobe (CaM_{12}) or C lobe (CaM_{34}) have been instrumental in revealing CaM lobe-specific modulation of Ca_v1 and Ca_v2 channels (Ben-Johny and Yue, 2014). To determine if CaM is involved in CDEA, we cotransfected $Ca_v1.4\Delta ex47$ with either CaM_{12} or CaM_{34}. While CaM_{34} did not affect $Ca_v1.4\Delta ex47$ current density, or cause alterations in I–V or tail I–V parameters that were specific for I_{Ca} (Fig. 2; and Tables 1 and 2), there was a

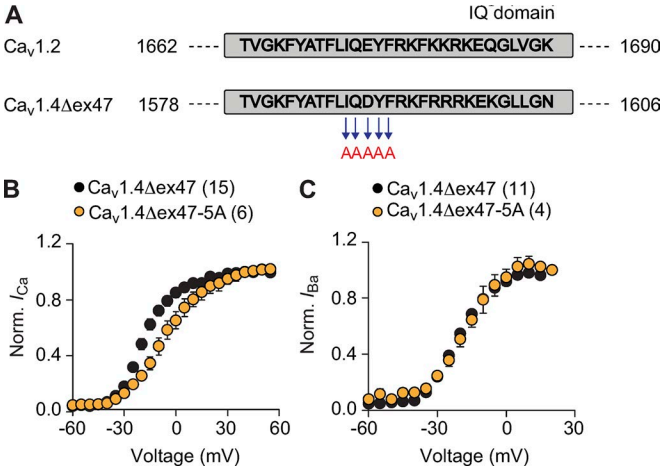

Figure 4. **IQ domain mutations blunt CDEA of $Ca_v1.4\Delta ex47$. (A)** Alignment of IQ domains of $Ca_v1.2$ and $Ca_v1.4\Delta ex47$ showing location of I1588A, Q1589A, D1590A, Y1591A, and F1592A in $Ca_v1.4\Delta ex47$ that were mutated to alanines $Ca_v1.4\Delta ex47$-5A. **(B and C)** Same as in Fig. 2 C except in cells transfected with $Ca_v1.4\Delta ex47$ (B) or $Ca_v1.4\Delta ex47$-5A (C). Error bars represent mean ± SEM.

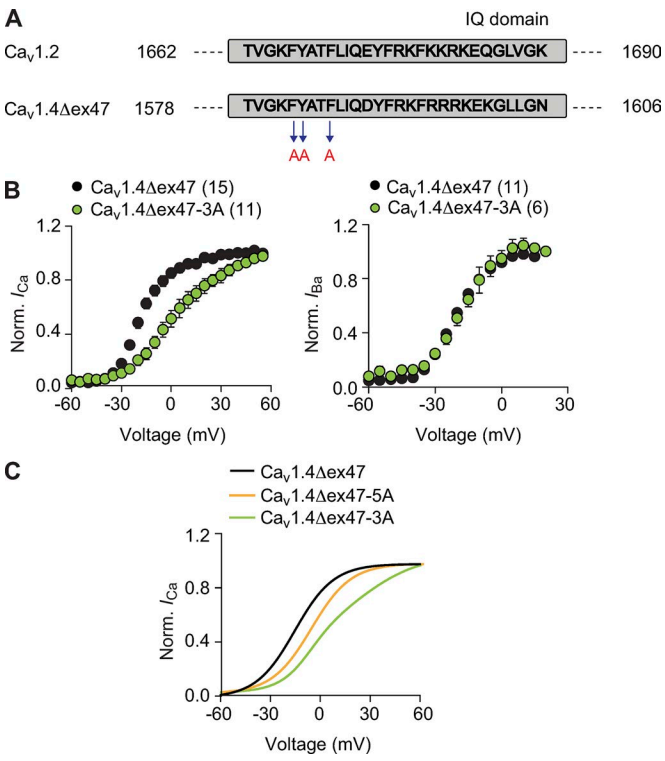

Figure 5. **Mutations of conserved aromatic residues prevents CDEA of $Ca_v1.4\Delta ex47$. (A)** Alignment of IQ domain showing location of F1582A, Y1583A, and F1586A in $Ca_v1.4\Delta ex47$, which were mutated to alanine in $Ca_v1.4\Delta ex47$-3A. **(B)** Same as in Fig. 2 C except for in cells transfected with $Ca_v1.4\Delta ex47$ or $Ca_v1.4\Delta ex47$-3A. **(C)** Boltzmann fits of the averaged data for I_{Ca} in B (single Boltzmann fit for $Ca_v1.4\Delta ex47$ and double Boltzmann fit for $Ca_v1.4\Delta ex47$-3A). The single Boltzmann fit of data in Fig. 4 B for $Ca_v1.4\Delta ex47$-5A I_{Ca} is overlaid for comparison. Error bars represent mean ± SEM.

significant decrease in current density and positive shift in V_h in the I–V curve in cells cotransfected with $Ca_v1.4\Delta ex47$ and CaM_{12} for I_{Ca}, and these alterations were not observed for I_{Ba} (Fig. 3, A and B; and Table 1). Coexpression of CaM_{12} also caused a positive shift in the tail I–V relationship only for I_{Ca} and not I_{Ba} (Fig. 3 C). Unlike for $Ca_v1.4\Delta ex47$ transfected alone or with CaM_{34} (Table 2), the tail I–V for I_{Ca} in cells cotransfected with CaM_{12} was best fit with a double Boltzmann function (Fig. 3 D and Table 3) with a decline in channel availability over voltages that paralleled the enhanced activation of I_{Ca} mediated by $Ca_v1.4\Delta ex47$ compared with $Ca_v1.4$ + ex47 (Fig. 1 B). There was also no impact of either CaM_{12} or CaM_{34} on the I–V or tail I–V relationship for $Ca_v1.4$ + ex47 (Fig. S1), demonstrating that this effect of CaM_{12} is specific for channels lacking exon 47. Collectively, our results show that deletion of exon 47 not only enhances voltage-dependent activation of I_{Ba} but also enables CDEA that involves the N lobe of CaM.

In $Ca_v1.4$, CaM binds to a consensus IQ domain in the pCTD of Ca_v1 channels (see Fig. 5 A). Mutation of the initial 5 amino acids within this domain (IQDYF) to alanine abolishes the binding of CaM to $Ca_v1.4$ (Griessmeier et al., 2009). Assuming that the 5A mutations would also disrupt CaM modulation of $Ca_v1.4\Delta ex47$, we introduced these mutations (I1588A, Q1589A, D1590A, Y1591A, and F1592A) into $Ca_v1.4\Delta ex47$ ($Ca_v1.4\Delta ex47$-5A; Fig. 4 A) and tested their involvement in CDEA. In Boltzmann fits of the tail I–V curves for $Ca_v1.4\Delta ex47$-5A, V_h was significantly more positive, and k shallower, than that for $Ca_v1.4\Delta ex47$. These alterations were seen for I_{Ca} and not for I_{Ba} mediated by $Ca_v1.4\Delta ex47$-5A (Fig. 4, B and C; and Table 2), indicating the importance of the IQ domain for CDEA of I_{Ca} but not voltage-dependent activation of I_{Ba}. To further probe the molecular determinants underlying CDEA, we focused on three aromatic residues that were shown to mediate CaM N lobe interactions with $Ca_v1.2$ (F1618A, Y1619A, F1622A; Van Petegem et al., 2005). Although there are differences in the residues surrounding the IQ domain of $Ca_v1.4$ and $Ca_v1.2$, these residues are conserved in $Ca_v1.4$ (F1582A, Y1583A, and F1586A; Fig. 5 A). Therefore, we reasoned that mutations of these residues might disrupt CaM N lobe regulation of CDEA. Consistent with this possibility, the 3A mutations in $Ca_v1.4\Delta ex47$ ($Ca_v1.4\Delta ex47$-3A) reversed the negative shift in V_h for I_{Ca} (Fig. 5 B; and Tables 2 and 3). Moreover, the tail I–V relationship of I_{Ca} for $Ca_v1.4\Delta ex47$-3A was best fit by a double Boltzmann equation (Fig. 5 C) with no significant differences in fit parameters compared with those obtained for $Ca_v1.4\Delta ex47$ cotransfected with CaM_{12} (Table 3). Compared with $Ca_v1.4\Delta ex47$, the positive shift in the tail I–V curve for I_{Ca} mediated by $Ca_v1.4\Delta ex47$-5A (Fig. 4 B)

Table 3. **Parameters for voltage-dependent activation from tail I–V data for $Ca_v1.4ex47$ + CaM_{12} and $Ca_v1.4ex47$-3A**

	$Ca_v1.4ex47$ + CaM_{12}	$Ca_v1.4ex47$-3A	P value
V_{h1} (mV)	−11 ± 2.2	−7 ± 2.0	0.129[a]
V_{h2} (mV)	0.02 ± 0.01	0.02 ± 0.02	0.942[b]
k_1	−7 ± 1.0	−8 ± 1.3	0.762[a]
k_2	−24 ± 7.2	−22 ± 5.0	0.767[a]

V_h and k values (mean ± SEM) were determined from double-Boltzmann fits of the tail I–V data as indicated in the "Methods" section.
[a]Student's t test.
[b]Mann–Whitney test.

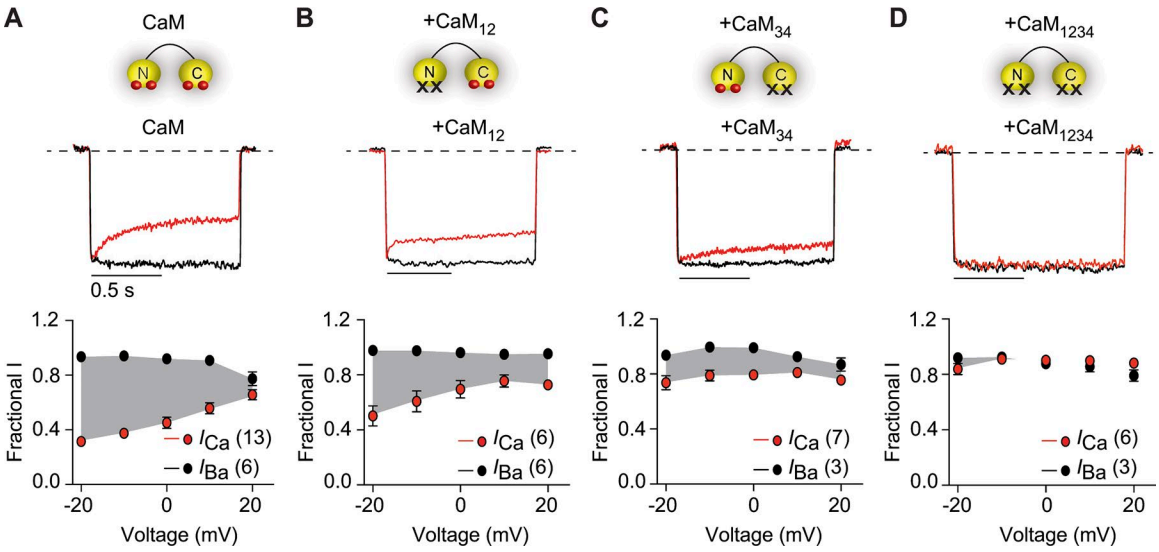

Figure 6. **CDI of $Ca_v1.4\Delta ex47$ depends on both the CaM N and C lobe. (A–D)** Representative traces for I_{Ca} (red) and I_{Ba} (black) evoked by 1-s pulse from −80 to −20 mV in cells transfected with $Ca_v1.4\Delta ex47$ alone (modulated by endogenous CaM; A) or cotransfected with CaM_{12} (B), CaM_{34} (C), or CaM_{1234} (D). In bottom graphs, currents were evoked by 1-s test pulses to various voltages. Fractional I represents current amplitude at the end of the pulse normalized to peak current amplitude and was plotted against test voltage. Gray shading reflects the extent of CDI. Error bars represent mean ± SEM.

was weaker than that for $Ca_v1.4\Delta ex47$-3A (Fig. 5 B), perhaps due to residual CaM N lobe modulation of $Ca_v1.4\Delta ex47$-5A. There was no effect of either 5A or 3A mutations on I_{Ba}, which further suggested that the enhanced voltage-dependent activation of I_{Ba} relies on distinct molecular determinants as compared with CDEA. Collectively, our results demonstrate that CaM N lobe mediates CDEA of $Ca_v1.4\Delta ex47$, which requires F1582A, Y1583A, and F1586A.

$Ca_v1.4\Delta ex47$ undergoes CDI that is mediated by both the N lobe and C lobe of CaM

In contrast to $Ca_v1.4$ + ex47, $Ca_v1.4\Delta ex47$ undergoes CDI that is evident as stronger inactivation of I_{Ca} as compared with I_{Ba} (Haeseleer et al., 2016). Previous analyses of $Ca_v1.3$ channels revealed the importance of the C lobe of CaM in mediating a rapid phase of CDI, whereas the N lobe mediates a slower component (Yang et al., 2006). To determine if this was also true for $Ca_v1.4\Delta ex47$, we tested the impact of CaM mutants on CDI of $Ca_v1.4\Delta ex47$. Inactivation of I_{Ca} and I_{Ba} was measured as the current amplitude at the end of a 1-s pulse normalized to the peak current amplitude (fractional I). Fractional Ca^{2+}-dependent inactivation was defined as the difference in fractional I_{Ca} and fractional I_{Ba} (F_{CDI}). In cells transfected with $Ca_v1.4\Delta ex47$ alone, I_{Ca} inactivation was greatest (smallest fractional I) at voltages on the rising phase of the I–V relationship (from −20 to 0 mV; Fig. 1 C), consistent with a role for Ca^{2+} influx during the test

Table 4. **Fractional CDI**

Construct	F_{CDI}	P value versus +ex47	P value versus Δex47	P value versus Δex47 + CaM_{12}	P value versus Δex47-3A
$Ca_v1.4$ + ex47	−0.19 ± 0.03	—	<0.001[a]	—	—
$Ca_v1.4\Delta ex47$	0.57 ± 0.03	—	—	—	—
$Ca_v1.4\Delta ex47$ + CaM_{12}	0.37 ± 0.07	<0.001[a]	0.008[a]	—	—
$Ca_v1.4\Delta ex47$ + CaM_{34}	0.22 ± 0.05	0.012[a]	<0.001[a]	0.171[a]	—
$Ca_v1.4\Delta ex47$ + CaM_{1234}	0.09 ± 0.05	0.530[a]	<0.001[a]	0.002[a]	—
$Ca_v1.4\Delta ex47$-5A	−0.12 ± 0.07	0.840[a]	<0.001[a]	—	—
$Ca_v1.4\Delta ex47$-3A	0.37 ± 0.13	0.004[a]	0.056[a]	—	—
$Ca_v1.4\Delta ex47$-3A + CaM_{34}	0.06 ± 0.01	—	—	—	0.044[b]

F_{CDI} values (mean ± SEM) were determined as indicated in the "Methods" section with the exception that for $Ca_v1.4\Delta ex47$ + CaM_{12}, F_{CDI} was measured at −10 mV to accommodate the positive shift in the tail-current voltage curves.
[a]One-way ANOVA with Tukey's multiple comparison test.
[b]Student's *t* test.

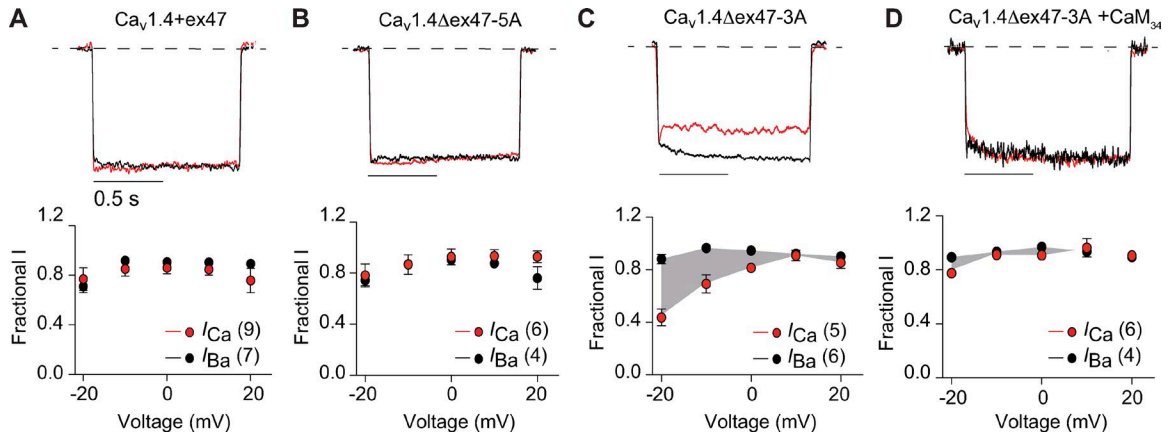

Figure 7. **$Ca_v1.4\Delta ex47$ 5A and 3A mutations differentially impact CDI. (A–D)** Same as in Fig. 6 except for cells transfected with $Ca_v1.4$ + ex47 (A), $Ca_v1.4\Delta ex47$-5A (B), $Ca_v1.4\Delta ex47$-3A (C), or $Ca_v1.4\Delta ex47$-3A + CaM_{34} (D). In C and D due to the slow activation of I_{Ba} (also I_{Ca} in D), the peak current was measured when the steady-state amplitude was reached at 500 ms. Error bars represent mean ± SEM.

pulse in promoting CDI. In contrast, I_{Ba} showed little inactivation across all voltages tested (Fig. 6 A). In cells cotransfected with CaM_{12} or CaM_{34}, Fractional I_{Ca} was still smaller than that for I_{Ba}, but to a lesser extent than in cells transfected with $Ca_v1.4\Delta ex47$ alone, such that F_{CDI} was significantly weaker with CaM_{12} and CaM_{34} than with $Ca_v1.4\Delta ex47$ alone (Fig. 6, B and C; and Table 4). To verify the importance of both lobes of CaM in regulating CDI, we analyzed the effects of a CaM mutant with both N and C lobes disabled (CaM_{1234}). There was no difference in fractional I_{Ca} and I_{Ba} in cells cotransfected with CaM_{1234}, indicating that CDI was abolished (Fig. 6 D and Table 4). These results show that CDI of $Ca_v1.4\Delta ex47$ is mediated by both the N and C lobe of CaM.

To investigate how molecular determinants in the IQ domain may influence CDI, we compared CDI in cells transfected with $Ca_v1.4\Delta ex47$-5A and $Ca_v1.4\Delta ex47$-3A. For $Ca_v1.4\Delta ex47$-5A, there was no CDI in that there was no difference in inactivation of I_{Ca} and I_{Ba}, similar to $Ca_v1.4$ + ex47 (Fig. 7, A and B; and Table 4). For $Ca_v1.4\Delta ex47$-3A, the results were more complex. In a subset of cells, there was no CDI, and I_{Ca} activated very slowly, likely reflecting the loss of CaM N lobe regulation of CDEA (Fig. S2).

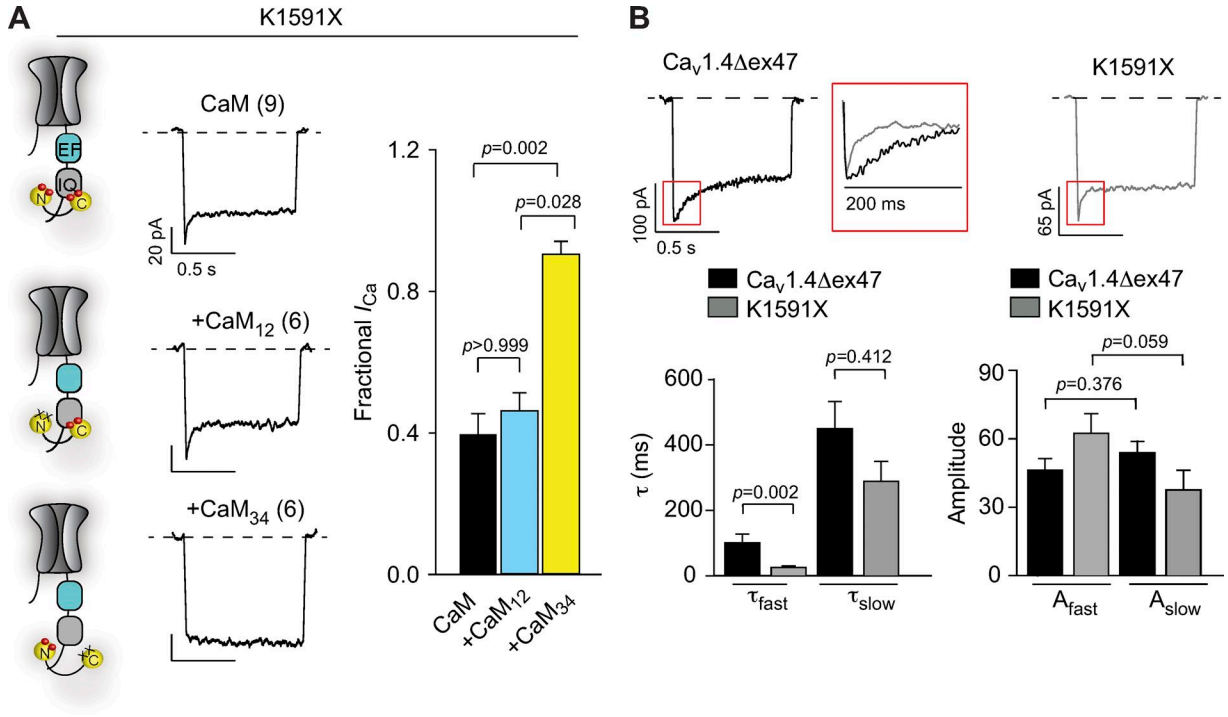

Figure 8. **K1591X CDI is mediated only by CaM C lobe. (A)** Representative traces and fractional I_{Ca} for I_{Ca} evoked by test pulse from −80 to −20 mV in cells transfected with K1591X alone or cotransfected with CaM_{12} or CaM_{34}. P values were determined by Kruskal–Wallis ANOVA followed by post hoc Dunn's multiple comparison test. **(B)** Representative traces for I_{Ca} evoked by −20 mV pulse in cells transfected with $Ca_v1.4\Delta ex47$ or K1591X. Inset shows superimposed I_{Ca} for $Ca_v1.4\Delta ex47$ (black) and K1591X (gray) on expanded time scale. Bottom graphs show averaged data for time constants (τ_{fast} and τ_{slow}) and amplitudes (A_{fast} and A_{slow}) obtained from double-exponential fits of I_{Ca} evoked as in A. P values were determined by Mann–Whitney test. Error bars represent mean ± SEM.

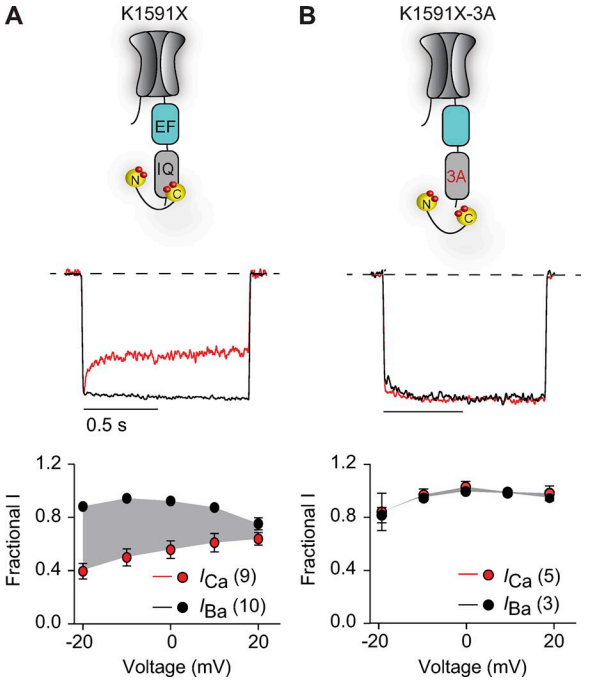

Figure 9. **3A mutations abolish CDI of K1591X. (A and B)** Same as in Fig. 7 but in cells transfected with K1591X (A) or K1591X-3A (B). Error bars represent mean ± SEM.

The lack of inactivation of both I_{Ca} and I_{Ba} in these cells suggests that the 3A mutations weaken CaM C lobe as well as CaM N lobe contributions to CDI. However, in some cells, there was residual CDI (Fig. 7 C), perhaps due to higher concentrations of CaM (Liu et al., 2010). In these cells, the fast phase of I_{Ca} inactivation was similar to that in cells cotransfected with $Ca_v1.4\Delta ex47$ and CaM_{12} (Fig. 6 B), suggesting that it was mediated by the CaM C lobe. Consistent with this possibility, cotransfection of $Ca_v1.4\Delta ex47$-3A with CaM_{34} eliminated CDI in all cells analyzed (Fig. 7 D and Table 4). We interpret these findings to mean that the 3A mutations in $Ca_v1.4\Delta ex47$ disrupt CaM N lobe–mediated CDI, but also weaken CaM C lobe–mediated CDI under some conditions.

CaM N lobe regulation of CDI is diminished with a CSNB2 mutation in $Ca_v1.4$

Although it responds to more global elevations in cytosolic Ca^{2+} with respect to CDI of Ca_v2 channels (DeMaria et al., 2001; Lee et al., 2003), the N lobe of CaM is a local Ca^{2+} sensor in the context of $Ca_v1.2$ and $Ca_v1.3$ CDI due to CaM binding to an N-terminal spatial Ca^{2+} transforming element (NSCaTE) in these channels. Thus, CaM N lobe–triggered CDI can be measured even with strong Ca^{2+} buffering (i.e., 5–10 mM EGTA) when $Ca_v1.2$ and $Ca_v1.3$ are coexpressed with CaM_{34} (Dick et al., 2008). The NSCaTE is not conserved in $Ca_v1.4$, and yet CaM N lobe–mediated CDI of $Ca_v1.4\Delta ex47$ (i.e., $+CaM_{34}$; Fig. 6 C) was still evident under our experimental conditions with 5 mM EGTA in the intracellular recording solution. We hypothesized that while deletion of exon 47 might disrupt the CTM's ability to blunt CaM interactions with the channel, the CTM and/or the rest of the C-terminal domain might enable CaM N lobe–mediated CDI even in the presence of high intracellular Ca^{2+} buffering. If so, then deletion of these C-terminal regions should prevent CaM N lobe–driven CDI.

To test this, we turned to the K1591X mutation associated with CSNB2 (Strom et al., 1998). This mutation truncates the entire CTD of $Ca_v1.4$ distal to the IQ domain (Fig. 8 A); the loss of the CTM enables CaM-dependent CDI (Singh et al., 2006). In contrast to the suppression of CDI of $Ca_v1.4\Delta ex47$ caused by both CaM_{12} and CaM_{34} (Fig. 6, B and C), I_{Ca} inactivation in K1591X mutant channels was suppressed by CaM_{34} but unaffected by CaM_{12}. Moreover, CaM_{34} completely abolished inactivation of I_{Ca} mediated by K1591X channels (Fig. 8 A), whereas CaM_{34} had a more modest impact in this respect for $Ca_v1.4\Delta ex47$ (Fig. 6 C). I_{Ca} in cells transfected with K1591X alone or together with CaM_{12} showed a rapid initial phase of inactivation that was abolished in cells cotransfected with K1591X and CaM_{34} (Fig. 8 A), similar to the CaM C lobe–mediated CDI of $Ca_v1.4\Delta ex47$ (i.e., $+CaM_{12}$; Fig. 6 B). For both K1591X and $Ca_v1.4\Delta ex47$, I_{Ca} could be fit with a double exponential function. However, the time constant (τ) for fast inactivation was significantly shorter for K1591X than for $Ca_v1.4\Delta ex47$ (Fig. 8 B). There was no significant difference in the amplitude of slow (A_{slow}) and fast (A_{fast}) inactivation for $Ca_v1.4\Delta ex47$, but A_{fast} was generally larger than that for A_{slow} for K1591X, although the difference did not reach statistical significance. These results show that K1591X is incapable of CaM N lobe–mediated CDI, and that the CaM C lobe mediates a fast phase of CDI that is more prominent in K1591X than in $Ca_v1.4\Delta ex47$.

We also analyzed the impact of the 3A mutations in K1591X (K1591X-3A). In contrast to the mixed effects of these mutations in weakening CDI of $Ca_v1.4\Delta ex47$ (Fig. 7, C and D; and Fig. S2), CDI

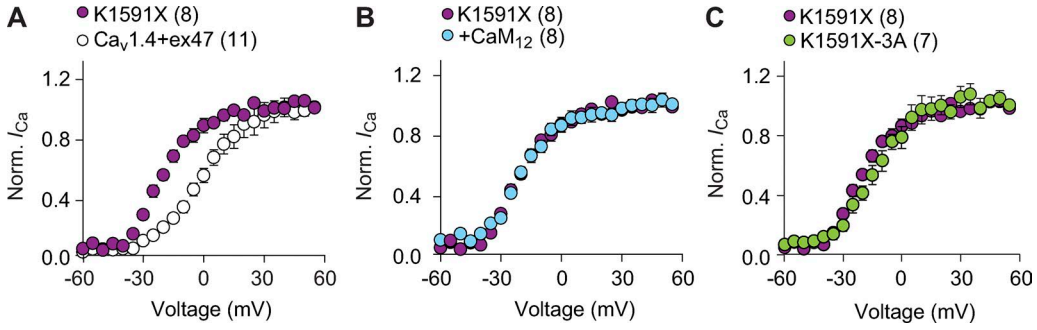

Figure 10. **Enhanced activation of *ICa* of K1591X is not mediated by CaM. (A–C)** Normalized tail I_{Ca}-voltage curves obtained as in Fig. 1 B in cells transfected with $Ca_v1.4$ + ex47 (A), and K1591X alone or cotransfected with CaM_{12} (B), or with K1591X-3A alone (C). Error bars represent mean ± SEM.

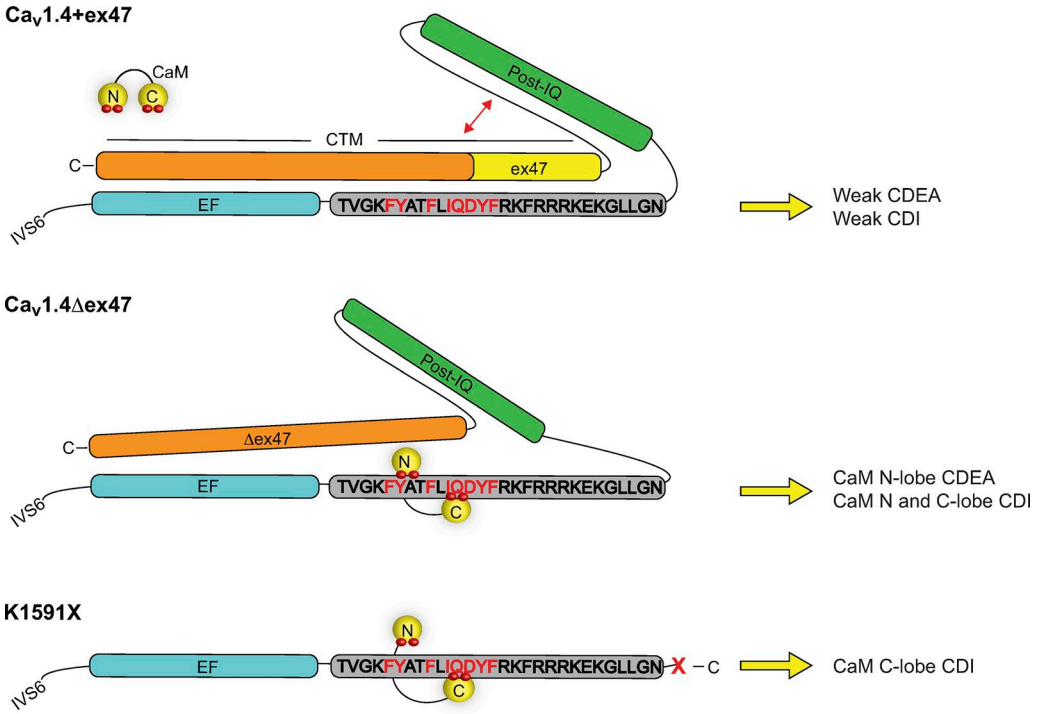

Figure 11. **Model for how variations in CTM may affect CaM interactions with the pCT.** The CTD of $Ca_v1.4$ is comprised of an EF-hand domain (EF, shaded blue), IQ domain (shaded gray), post-IQ domain (Post-IQ, shaded green) containing proximal C-terminal regulatory domain required for CTM modulation (Singh et al., 2006), and CTM (shaded orange) containing exon 47 (shaded yellow). Top: The CTM of $Ca_v1.4$ + ex47 channels suppresses CDEA and CDI through interactions with the proximal C-terminal regulatory domain within the post-IQ region, which competes with CaM for binding to the IQ domain. Middle: Deletion of exon 47 from the CTM of $Ca_v1.4\Delta ex47$ allows CaM N and C lobe interactions that support CDI, with the CaM N lobe interaction also promoting CDEA. The CaM N lobe contacts may be stabilized by the residual CTM (and/or post-IQ domain) in $Ca_v1.4\Delta ex47$. Bottom: The complete absence of the CTM and/or pre-IQ domain in K1591X allows robust modulation of CDI only by CaM C lobe.

was completely abolished in all recordings of cells transfected with K1591X-3A (Fig. 9, A and B; F_{CDI} = 0.47 ± 0.04 for K1591X versus −0.04 ± 0.03 for K1591X-3A; P = 0.001 by *t* test). These results reveal a more prominent role for F1582A, Y1583A, and F1586A in CaM C lobe–mediated CDI of K1591X as compared with $Ca_v1.4\Delta ex47$.

Given that K1591X is deficient in CaM N lobe–dependent CDI, we tested if this mutant was also lacking in CaM N lobe regulation of CDEA. If so, then the tail current I–V relationship for I_{Ca} should not be affected by coexpression with CaM_{12} or by the 3A mutations. As shown previously with different combinations of auxiliary subunits than those used here (Singh et al., 2006), K1591X exhibited a negative shift in activation of I_{Ca} compared with wild-type $Ca_v1.4$ + ex47 (Fig. 10 A and Table 2). Unlike $Ca_v1.4\Delta ex47$, I_{Ca} mediated by K1591X was unaffected by CaM_{12} or the 3A mutations (Fig. 10, B and C); there was no significant difference in the V_h or *k* for K1591X transfected alone or with CaM_{12}, or for K1591X and K1591X-3A (Table 2). Thus, although F1582A, Y1583A, and F1586A regulate CaM C lobe–dependent CDI, these residues are dispensable for regulating activation of K1591X.

Discussion

Our study provides new insights into the regulation of Ca_v channels by CaM. First, we identify an unexpected role for CaM in CDEA—a Ca^{2+}-dependent enhancement of $Ca_v1.4$ activation mediated by the N lobe of CaM. CDEA requires the deletion of exon 47 as well as the inclusion of other regions of the CTD in $Ca_v1.4\Delta ex47$; the absence of these regions in K1591X may account for its lack of CaM N lobe–mediated CDEA. Second, we show that when CDI of $Ca_v1.4$ is unmasked by partial disruption of the CTM, CaM N lobe mediates a slow component of CDI that is significantly weakened upon full deletion of CTD distal to the IQ domain. This contribution of CaM N lobe is evident in CDI of $Ca_v1.4\Delta ex47$ but not that of K1591X, which is dominated by the CaM C lobe. Our findings support a model in which variations in the CTD adjust how the N and C lobe of CaM modulate $Ca_v1.4$ (Fig. 11), providing a context for understanding the functional consequences of naturally occurring and pathological variants of $Ca_v1.4$ in the retina.

A novel role for CaM in enhancing activation of $Ca_v1.4$

CaM is a dynamic regulator of Ca_v channels and can vary its modulatory impact upon binding Ca^{2+}. When bound to the pCTD, Ca^{2+}-free (apo) CaM boosts channel open probability (P_o), which then diminishes as Ca^{2+} binding to CaM triggers CDI (Adams et al., 2014). In the context of $Ca_v1.4$ + ex47 and the long variant of $Ca_v1.3$ (+exon 42A; Singh et al., 2008), the CTM competes with apoCaM binding (Liu et al., 2010; Adams et al., 2014). Deletion of exon 47 may allow for stronger binding of apoCaM to the pCTD,

which may explain the negative shifts in the tail I–V curves for I_{Ba} mediated by $Ca_v1.4\Delta ex47$ (Fig. 1 C). While these shifts were not affected by CaM mutants (Figs. 2 C and 3 C) or by the 3A or 5A mutations (Figs. 4 C and 5 C), it is possible that these experimental manipulations incompletely blunted apoCaM interactions with the channel, as some determinants for apoCaM binding may reside outside the IQ domain (Ben Johny et al., 2013). As has been proposed for Ca^{2+}/CaM-dependent facilitation of $Ca_v2.1$ channels (Chaudhuri et al., 2007), Ca^{2+}/CaM may promote transitions to a gating mode characterized by even higher P_o than with apoCaM, and this may be disrupted by the 3A and 5A mutations. Finer resolution of the mechanism by which the CTM modulates activation of I_{Ca} and I_{Ba} awaits detailed alanine scanning mutagenesis to unearth specific contacts for CaM in the pCTD in combination with single-channel analyses of P_o.

Differences in the CaM lobe dependence of $Ca_v1.4\Delta ex47$ and K1591X

Unlike $Ca_v1.4\Delta ex47$, K1591X does not undergo CDEA in that neither CaM N lobe nor the 3A mutations had any effects on the tail I–V curves for I_{Ca} (Fig. 10). The absence of CaM N lobe regulation of K1591X is further suggested by our kinetic analyses of I_{Ca} inactivation, as well as the blockade of CDI by CaM_{34} (Fig. 8 A). These experiments implicated the CaM C lobe in mediating CDI of K1591X, in stark contrast to the contributions of both CaM lobes to CDI of $Ca_v1.4\Delta ex47$ (Fig. 6). Deletion of exon 47 removes the initial 47 amino acids of the CTM (Singh et al., 2006), 26 residues according to the CTM region defined by Wahl-Schott et al. (2006). However, $Ca_v1.4\Delta ex47$ still possesses a 34–amino acid stretch within the CTM shown to be critical for CDI suppression (Singh et al., 2006; Wahl-Schott et al., 2006). We propose that the residual CTM in concert with the post-IQ region unmasks and/or stabilizes CaM N lobe contacts within the IQ domain that support the slow component of CDI in $Ca_v1.4\Delta ex47$ (Fig. 11), which is blocked by CaM_{12} (and by 3A mutations; Figs. 6 B and 7 C). In the context of $Ca_v1.2$, thephenylalanine, tyrosine, and phenylalanine residues affected by the 3A mutations form extensive contacts with CaM N lobe (Van Petegem et al., 2005). Since these residues are conserved in $Ca_v1.4$, as well as in all Ca_v1 channels (Van Petegem et al., 2005), we propose that they may similarly serve as anchoring points for CaM N lobe in $Ca_v1.4\Delta ex47$. Although these residues may be free to interact with CaM in K1591X, the absence of both CTM and post-IQ regions in K1591X may prevent the CaM N lobe interaction, or its functional consequences in promoting CDI (Fig. 11). However, our findings also reveal a key role for F1582A, Y1583A, and F1586A in weakening CaM C lobe–mediated CDI in both $Ca_v1.4\Delta ex47$ and K1591X, which is not wholly unexpected given that CaM C lobe contacts may be intermingled among these residues (Van Petegem et al., 2005). Additional structural studies are needed to resolve how the CTM with and without exon 47 affects CaM interactions with the pCTD.

Physiological relevance of $Ca_v1.4$ CTM modifications

Although our results suggest differences in CaM regulation of $Ca_v1.4\Delta ex47$ and K1591X, the impact of CaM on these channels in photoreceptors is likely influenced by CaBP4 (Haeseleer et al., 2004; Lee et al., 2015)—a member of a family of Ca^{2+} binding proteins (CaBPs) that suppress CDI of Ca_v1 channels in part by competing with CaM binding to the IQ domain (Hardie and Lee, 2016). CaBP4 binds to the same sites as CaM within the pCTD of $Ca_v1.4$ (Shaltiel et al., 2012; Haeseleer et al., 2016), and suppresses but does not completely abolish CDI of $Ca_v1.4\Delta ex47$ (Haeseleer et al., 2016). This suggests that CaM may still interact with and modulate $Ca_v1.4\Delta ex47$ despite the presence of CaBP4 in photoreceptor synaptic terminals (Haeseleer et al., 2004; Lee et al., 2015). When bound to Ca^{2+}, CaM is expected to compete more effectively for binding to the Ca_v1 IQ domain than CaBPs (Findeisen et al., 2013), and CaBPs can bind to sites other than the IQ domain in regulating CDI (Zhou et al., 2005; Yang et al., 2014). Fluctuations in presynaptic Ca^{2+} levels may promote dynamic regulation of $Ca_v1.4\Delta ex47$ by CaM and CaBP4, allowing for CDEA and CDI to shape presynaptic Ca^{2+} signals supporting glutamate release from photoreceptor terminals. If K1591X is similarly regulated by CaM, the lack of CaM N lobe regulation of CDEA and CDI may lead to aberrant regulation of Ca^{2+} signals that could degrade the transmission of visual information. Considering that the CTD of Ca_v channels is a hotspot for protein interactions (Calin-Jageman and Lee, 2008), it is also conceivable that K1591X is unable to assemble with key synaptic proteins needed for the proper localization and/or function of the channel in photoreceptors.

Acknowledgments

This work was supported by the National Institutes of Health (DC009433, NS084190, and EY026817 to A. Lee and EY026477 to B. Williams), the Neuroscience Training Program (T32 NS007421), a Carver Research Program of Excellence Award, and the University of Iowa's Bioscience Academy (R25GM058939).

The authors declare no competing financial interests.

Author contributions: B. Williams conducted the research. B. Williams, F. Haeseleer, and A. Lee contributed to experimental design. B. Williams and A. Lee wrote the paper.

Richard W. Aldrich served as editor.

Submitted: 31 May 2018
Accepted: 3 October 2018

References

Adams, P.J., E. Garcia, L.S. David, K.J. Mulatz, S.D. Spacey, and T.P. Snutch. 2009. Ca(V)2.1 P/Q-type calcium channel alternative splicing affects the functional impact of familial hemiplegic migraine mutations: implications for calcium channelopathies. *Channels (Austin)*. 3:110–121. https://doi.org/10.4161/chan.3.2.7932

Adams, P.J., M. Ben-Johny, I.E. Dick, T. Inoue, and D.T. Yue. 2014. Apocalmodulin itself promotes ion channel opening and Ca(2+) regulation. *Cell*. 159:608–622. https://doi.org/10.1016/j.cell.2014.09.047

Andrade, A., S. Denome, Y.Q. Jiang, S. Marangoudakis, and D. Lipscombe. 2010. Opioid inhibition of N-type Ca2+ channels and spinal analgesia couple to alternative splicing. *Nat. Neurosci.* 13:1249–1256. https://doi.org/10.1038/nn.2643

Baumann, L., A. Gerstner, X. Zong, M. Biel, and C. Wahl-Schott. 2004. Functional characterization of the L-type Ca2+ channel Cav1.4alpha1 from mouse retina. *Invest. Ophthalmol. Vis. Sci.* 45:708–713. https://doi.org/10.1167/iovs.03-0937

Ben Johny, M., P.S. Yang, H. Bazzazi, and D.T. Yue. 2013. Dynamic switching of calmodulin interactions underlies Ca2+ regulation of CaV1.3 channels. *Nat. Commun.* 4:1717. https://doi.org/10.1038/ncomms2727

Ben-Johny, M., and D.T. Yue. 2014. Calmodulin regulation (calmodulation) of voltage-gated calcium channels. *J. Gen. Physiol.* 143:679–692. https://doi.org/10.1085/jgp.201311153

Buraei, Z., and J. Yang. 2013. Structure and function of the β subunit of voltage-gated Ca^{2+} channels. *Biochim. Biophys. Acta.* 1828:1530–1540. https://doi.org/10.1016/j.bbamem.2012.08.028

Calin-Jageman, I., and A. Lee. 2008. Ca(v)1 L-type Ca^{2+} channel signaling complexes in neurons. *J. Neurochem.* 105:573–583. https://doi.org/10.1111/j.1471-4159.2008.05286.x

Chaudhuri, D., S.Y. Chang, C.D. DeMaria, R.S. Alvania, T.W. Soong, and D.T. Yue. 2004. Alternative splicing as a molecular switch for Ca^{2+}/calmodulin-dependent facilitation of P/Q-type Ca^{2+} channels. *J. Neurosci.* 24:6334–6342. https://doi.org/10.1523/JNEUROSCI.1712-04.2004

Chaudhuri, D., B.A. Alseikhan, S.Y. Chang, T.W. Soong, and D.T. Yue. 2005. Developmental activation of calmodulin-dependent facilitation of cerebellar P-type Ca^{2+} current. *J. Neurosci.* 25:8282–8294. https://doi.org/10.1523/JNEUROSCI.2253-05.2005

Chaudhuri, D., J.B. Issa, and D.T. Yue. 2007. Elementary mechanisms producing facilitation of $Ca_v2.1$ (P/Q-type) channels. *J. Gen. Physiol.* 129:385–401. https://doi.org/10.1085/jgp.200709749

DeMaria, C.D., T.W. Soong, B.A. Alseikhan, R.S. Alvania, and D.T. Yue. 2001. Calmodulin bifurcates the local Ca^{2+} signal that modulates P/Q-type Ca^{2+} channels. *Nature.* 411:484–489. https://doi.org/10.1038/35078091

Dick, I.E., M.R. Tadross, H. Liang, L.H. Tay, W. Yang, and D.T. Yue. 2008. A modular switch for spatial Ca2+ selectivity in the calmodulin regulation of CaV channels. *Nature.* 451:830–834. https://doi.org/10.1038/nature06529

Dolphin, A.C. 2013. The α2δ subunits of voltage-gated calcium channels. *Biochim. Biophys. Acta.* 1828:1541–1549. https://doi.org/10.1016/j.bbamem.2012.11.019

Findeisen, F., C.H. Rumpf, and D.L. Minor Jr. 2013. Apo states of calmodulin and CaBP1 control CaV1 voltage-gated calcium channel function through direct competition for the IQ domain. *J. Mol. Biol.* 425:3217–3234. https://doi.org/10.1016/j.jmb.2013.06.024

Griessmeier, K., H. Cuny, K. Rötzer, O. Griesbeck, H. Harz, M. Biel, and C. Wahl-Schott. 2009. Calmodulin is a functional regulator of $Ca_v1.4$ L-type Ca^{2+} channels. *J. Biol. Chem.* 284:29809–29816. https://doi.org/10.1074/jbc.M109.048082

Haeseleer, F., Y. Imanishi, T. Maeda, D.E. Possin, A. Maeda, A. Lee, F. Rieke, and K. Palczewski. 2004. Essential role of Ca^{2+}-binding protein 4, a $Ca_v1.4$ channel regulator, in photoreceptor synaptic function. *Nat. Neurosci.* 7:1079–1087. https://doi.org/10.1038/nn1320

Haeseleer, F., B. Williams, and A. Lee. 2016. Characterization of C-terminal Splice Variants of $Ca_v1.4$ Ca^{2+} Channels in Human Retina. *J. Biol. Chem.* 291:15663–15673. https://doi.org/10.1074/jbc.M116.731737

Hardie, J., and A. Lee. 2016. Decalmodulation of Cav1 channels by CaBPs. *Channels (Austin).* 10:33–37. https://doi.org/10.1080/19336950.2015.1051273

Lee, A., H. Zhou, T. Scheuer, and W.A. Catterall. 2003. Molecular determinants of $Ca^{(2+)}$/calmodulin-dependent regulation of Ca(v)2.1 channels. *Proc. Natl. Acad. Sci. USA.* 100:16059–16064. https://doi.org/10.1073/pnas.2237000100

Lee, A., S. Wang, B. Williams, J. Hagen, T.E. Scheetz, and F. Haeseleer. 2015. Characterization of Cav1.4 complexes ($\alpha_1$1.4, β_2, and $\alpha_2\delta$4) in HEK293T cells and in the retina. *J. Biol. Chem.* 290:1505–1521. https://doi.org/10.1074/jbc.M114.607465

Lipscombe, D., S.E. Allen, and C.P. Toro. 2013. Control of neuronal voltage-gated calcium ion channels from RNA to protein. *Trends Neurosci.* 36:598–609. https://doi.org/10.1016/j.tins.2013.06.008

Liu, X., P.S. Yang, W. Yang, and D.T. Yue. 2010. Enzyme-inhibitor-like tuning of Ca(2+) channel connectivity with calmodulin. *Nature.* 463:968–972. https://doi.org/10.1038/nature08766

Liu, X., V. Kerov, F. Haeseleer, A. Majumder, N. Artemyev, S.A. Baker, and A. Lee. 2013. Dysregulation of Ca(v)1.4 channels disrupts the maturation of photoreceptor synaptic ribbons in congenital stationary night blindness type 2. *Channels (Austin).* 7:514–523. https://doi.org/10.4161/chan.26376

Mansergh, F., N.C. Orton, J.P. Vessey, M.R. Lalonde, W.K. Stell, F. Tremblay, S. Barnes, D.E. Rancourt, and N.T. Bech-Hansen. 2005. Mutation of the calcium channel gene Cacna1f disrupts calcium signaling, synaptic transmission and cellular organization in mouse retina. *Hum. Mol. Genet.* 14:3035–3046. https://doi.org/10.1093/hmg/ddi336

McRory, J.E., J. Hamid, C.J. Doering, E. Garcia, R. Parker, K. Hamming, L. Chen, M. Hildebrand, A.M. Beedle, L. Feldcamp, et al. 2004. The CACNA1F gene encodes an L-type calcium channel with unique biophysical properties and tissue distribution. *J. Neurosci.* 24:1707–1718. https://doi.org/10.1523/JNEUROSCI.4846-03.2004

Peterson, B.Z., C.D. DeMaria, J.P. Adelman, and D.T. Yue. 1999. Calmodulin is the Ca^{2+} sensor for Ca^{2+} -dependent inactivation of L-type calcium channels. *Neuron.* 22:549–558. https://doi.org/10.1016/S0896-6273(00)80709-6

Raingo, J., A.J. Castiglioni, and D. Lipscombe. 2007. Alternative splicing controls G protein-dependent inhibition of N-type calcium channels in nociceptors. *Nat. Neurosci.* 10:285–292. https://doi.org/10.1038/nn1848

Shaltiel, L., C. Paparizos, S. Fenske, S. Hassan, C. Gruner, K. Rötzer, M. Biel, and C.A. Wahl-Schott. 2012. Complex regulation of voltage-dependent activation and inactivation properties of retinal voltage-gated $Ca_v1.4$ L-type Ca^{2+} channels by Ca^{2+}-binding protein 4 (CaBP4). *J. Biol. Chem.* 287:36312–36321. https://doi.org/10.1074/jbc.M112.392811

Simms, B.A., and G.W. Zamponi. 2014. Neuronal voltage-gated calcium channels: structure, function, and dysfunction. *Neuron.* 82:24–45. https://doi.org/10.1016/j.neuron.2014.03.016

Singh, A., D. Hamedinger, J.C. Hoda, M. Gebhart, A. Koschak, C. Romanin, and J. Striessnig. 2006. C-terminal modulator controls Ca^{2+}-dependent gating of Ca(v)1.4 L-type Ca^{2+} channels. *Nat. Neurosci.* 9:1108–1116. https://doi.org/10.1038/nn1751

Singh, A., M. Gebhart, R. Fritsch, M.J. Sinnegger-Brauns, C. Poggiani, J.C. Hoda, J. Engel, C. Romanin, J. Striessnig, and A. Koschak. 2008. Modulation of voltage- and Ca2+-dependent gating of CaV1.3 L-type calcium channels by alternative splicing of a C-terminal regulatory domain. *J. Biol. Chem.* 283:20733–20744. https://doi.org/10.1074/jbc.M802254200

Specht, D., S.B. Wu, P. Turner, P. Dearden, F. Koentgen, U. Wolfrum, M. Maw, J.H. Brandstätter, and S. tom Dieck. 2009. Effects of presynaptic mutations on a postsynaptic Cacna1s calcium channel colocalized with mGluR6 at mouse photoreceptor ribbon synapses. *Invest. Ophthalmol. Vis. Sci.* 50:505–515. https://doi.org/10.1167/iovs.08-2758

Strom, T.M., G. Nyakatura, E. Apfelstedt-Sylla, H. Hellebrand, B. Lorenz, B.H.F. Weber, K. Wutz, N. Gutwillinger, K. Rüther, B. Drescher, et al. 1998. An L-type calcium-channel gene mutated in incomplete X-linked congenital stationary night blindness. *Nat. Genet.* 19:260–263. https://doi.org/10.1038/940

Tan, G.M., D. Yu, J. Wang, and T.W. Soong. 2012. Alternative splicing at C terminus of Ca(V)1.4 calcium channel modulates calcium-dependent inactivation, activation potential, and current density. *J. Biol. Chem.* 287:832–847. https://doi.org/10.1074/jbc.M111.268722

Van Petegem, F., F.C. Chatelain, and D.L.J. Minor Jr. 2005. Insights into voltage-gated calcium channel regulation from the structure of the $Ca_V1.2$ IQ domain-Ca^{2+}/calmodulin complex. *Nat. Struct. Mol. Biol.* 12:1108–1115. https://doi.org/10.1038/nsmb1027

Wahl-Schott, C., L. Baumann, H. Cuny, C. Eckert, K. Griessmeier, and M. Biel. 2006. Switching off calcium-dependent inactivation in L-type calcium channels by an autoinhibitory domain. *Proc. Natl. Acad. Sci. USA.* 103:15657–15662. https://doi.org/10.1073/pnas.0604621103

Yang, P.S., B.A. Alseikhan, H. Hiel, L. Grant, M.X. Mori, W. Yang, P.A. Fuchs, and D.T. Yue. 2006. Switching of Ca^{2+}-dependent inactivation of Ca(v)1.3 channels by calcium binding proteins of auditory hair cells. *J. Neurosci.* 26:10677–10689. https://doi.org/10.1523/JNEUROSCI.3236-06.2006

Yang, P.S., M.B. Johny, and D.T. Yue. 2014. Allostery in Ca^{2+} channel modulation by calcium-binding proteins. *Nat. Chem. Biol.* 10:231–238. https://doi.org/10.1038/nchembio.1436

Yu, F.H., V. Yarov-Yarovoy, G.A. Gutman, and W.A. Catterall. 2005. Overview of molecular relationships in the voltage-gated ion channel superfamily. *Pharmacol. Rev.* 57:387–395. https://doi.org/10.1124/pr.57.4.13

Zhou, H., K. Yu, K.L. McCoy, and A. Lee. 2005. Molecular mechanism for divergent regulation of $Ca_v1.2$ Ca^{2+} channels by calmodulin and Ca^{2+}-binding protein-1. *J. Biol. Chem.* 280:29612–29619. https://doi.org/10.1074/jbc.M504167200